

Nuclear magnetic resonance of ^{82}Br in hcp Co

G. Seewald, E. Hagn, and E. Zech

Physik-Department, Technische Universität München, D-85748 Garching, Germany

K. Freitag and P. Herzog

Institut für Strahlen- und Kernphysik, Universität Bonn, D-53115 Bonn, Germany

(Received 15 January 1999)

The static and dynamic hyperfine interactions of radioactive ^{82}Br in single-crystal hcp Co were measured with the techniques of nuclear magnetic resonance on oriented nuclei (NMR-ON), modulated adiabatic fast passage on oriented nuclei, and pulsed NMR-ON. The isotropic and anisotropic parts of the magnetic and electric hyperfine interaction with respect to the single-crystal c axis were determined. The principal component V_{zz} of the electric-field gradient tensor consists of an isotropic and an anisotropic part: $V_{zz}^{(\text{iso})}$ is small but nonzero; $V_{zz}^{(\text{ani})}$ has positive sign, in contrast to all other presently known impurity-hcp-Co systems for which $V_{zz}^{(\text{ani})}$ is negative. The nuclear spin-lattice relaxation is considerably faster than expected from known data on Y, Nb, and Zr in hcp Co. [S0163-1829(99)11621-7]

I. INTRODUCTION

The static hyperfine interaction at the nuclear site of atoms dissolved as dilute impurities in ferromagnetic hcp Co consists of two contributions: (i) the magnetic interaction of the nuclear magnetic moment μ with the magnetic hyperfine field B_{HF} ; (ii) the electric quadrupole interaction (EQI) of the nuclear spectroscopic quadrupole moment eQ with the electric-field gradient (EFG) V_{zz} at the site of the nucleus. The aim of investigations of the hyperfine interaction of impurity-hcp-Co systems has mainly been twofold: (i) study of electric quadrupole moments of radioactive nuclei utilizing the EFG in hcp Co (Refs. 1–4); (ii) study of the magnetic hyperfine field and the EFG in hcp Co.

For Fe and Ni as host lattice, the magnetic hyperfine field is known experimentally for most elements.⁵ The theoretical description has been improved considerably in the last few years; the theoretical hyperfine fields are in moderately good agreement with the experimental values.^{6–9} For hcp Co as host matrix, experimental information on the magnetic hyperfine fields is much less complete. This is due to the fact that it is very difficult to prepare dilute hcp-Co-based alloys by thermal methods because of the hcp-fcc phase transition of Co at $\sim 420^\circ\text{C}$. Thus, for investigations on impurity-hcp-Co systems, it is more appropriate to prepare samples by implantation techniques and to determine the hyperfine interaction with a radiation-based method. The NMR-ON (nuclear magnetic resonance on oriented nuclei) technique is well suited for that purpose, since practically for every element at least one suitable isotope exists on which NMR-ON can be observed.

For hcp Co, both the magnetic hyperfine field and the principal component of the EFG are anisotropic, i.e., they depend on the angle between the direction of the electronic magnetization M and the crystallographic c axis.

The EFG of Br in hcp Co has two interesting aspects: (i) It is known that for the pure system $\text{CoCo}^{(\text{hcp})}$ an isotropic contribution to the electric quadrupole interaction exists, originating from an EFG the principal z' axis of which

points along the direction of the magnetic hyperfine field. The existence of such an EFG has been ascribed to an unquenched orbital d moment arising from the spin-orbit interaction. We denote this type of EFG henceforth as spin-orbit EFG (SO-EFG). There is no information on the existence or nonexistence of a SO-EFG for a non- d -element in hcp Co. (ii) The anisotropic contribution to the electric quadrupole interaction is caused by the EFG originating from the non-cubic structure of the lattice. Here the Sternheimer (anti)sh-ielding factor enters, which depends on the electronic configuration at the impurity site. Depending on the electronic configuration at the Br site—which is unknown—the sign of the quadrupole interaction could be opposite to the “normal” sign: The principal component of the “anisotropic” EFG is negative for all impurity-hcp-Co systems that are presently known. Thus the experiment could also yield information on the core electronic configuration of the halogen bromine in the metal cobalt.

Therefore we investigated the system Br-hcp-Co with radiation-based NMR methods utilizing the radioactive isotope ^{82}Br .

II. HYPERFINE INTERACTION IN HCP Co

As function of the angle θ between the direction of the electronic magnetization M and the c axis of a hcp Co single crystal, the magnetic hyperfine field B_{HF} and the principal component V_{zz} of the traceless EFG tensor can in good approximation be described by

$$B_{\text{HF}}(\theta) = B_{\text{HF}}^{(\text{iso})} + B_{\text{HF}}^{(\text{ani})} P_2(\cos\theta), \quad (1)$$

$$V_{zz}(\theta) = V_{zz}^{(\text{iso})} + V_{zz}^{(\text{ani})} P_2(\cos\theta). \quad (2)$$

In the case of a combined magnetic-dipole plus electric-quadrupole hyperfine interaction the NMR signal consists of a set of $2I$ subresonances. These are located at

$$\nu_{m \rightarrow m+1} = \nu_{\text{mag}} - \Delta \nu_{\text{Q}}(m+1/2), \quad (3)$$

$$\nu_{\text{mag}} = \nu_{\text{M}}(\theta) + |g| \mu_{\text{N}} [B_{\text{ext}}(1 + K_{\text{s}}) \cos \theta - B_{\text{dem}}(\theta)] \text{sgn}(B_{\text{HF}}) / h, \quad (4)$$

$$\nu_{\text{M}}(\theta) = |g \mu_{\text{N}} B_{\text{HF}}(\theta) / h|, \quad (5)$$

$$\nu_{\text{Q}}(\theta) = eQV_{zz}(\theta), \quad (6)$$

$$\Delta \nu_{\text{Q}}(\theta) = 3\nu_{\text{Q}}(\theta) / [2I(2I-1)], \quad (7)$$

where ν_{M} and ν_{Q} are the magnetic hyperfine splitting frequency and the quadrupole interaction frequency, g and eQ are the nuclear g factor and the spectroscopic quadrupole moment, B_{ext} is the external magnetic field, K_{s} is the resonance shift parameter that includes Knight shift and diamagnetic shielding, $\text{sgn}(B_{\text{HF}})$ is the sign of B_{HF} with respect to B_{ext} , B_{dem} is the demagnetization field, and $\Delta \nu_{\text{Q}}$ is the quadrupole subresonance separation. (The demagnetization tensor can in good approximation be replaced by a set of sample-geometry-dependent main-axes demagnetization fields.)

If the quadrupole subresonance separation is small compared to the magnetic inhomogeneous broadening, the subresonances cannot be resolved. In this case there is an offset between the magnetic-resonance frequency and the center $\bar{\nu}$ of the observed resonance signal,

$$\bar{\nu} = \nu_{\text{mag}} - \Delta \nu_{\text{Q}}(\bar{m} + 1/2). \quad (8)$$

Here $(\bar{m} + 1/2)$ takes into account the weighted average of all subresonances, which depends mainly on the temperature T ; it can be calculated as outlined in Ref. 10.

III. MEASUREMENT TECHNIQUES

A. NMR-ON

In the NMR-ON method the resonant absorption of an applied radio frequency (rf) field is detected via nuclear radiation.¹¹ The angular distribution $W(\vartheta)$ and the anisotropy $A(\vartheta)$ of γ rays emitted in the decay of oriented nuclei at the temperature T is given by

$$A(\vartheta) = W(\vartheta) - 1 = \sum_{k \text{ even}} A_k B_k(a_m) P_k(\cos \vartheta) Q_k, \quad (9)$$

where all parameters have their conventional meaning.¹² In the present work the ratio of count rates at 0° and 90° ,

$$\epsilon = W(0^\circ) / W(90^\circ) - 1, \quad (10)$$

is analyzed, which is independent of the decreasing count rate due to the radioactive decay.

B. AFP-ON and MAPON

In the techniques of adiabatic fast passage on oriented nuclei (AFP-ON) and modulated adiabatic fast passage on oriented nuclei (MAPON) the rf is slowly and continuously swept through the resonance conditions. The interaction with the nuclear-spin system is detected via the γ anisotropy after the sweep (post-passage signal).

With AFP-ON on a quadrupole split system, cyclic permutation of the sublevel populations a_m is obtained. For a quadrupole-split system the final state after an AFP sweep is

strongly different for the two different rf sweep directions: The population of the first accessed sublevel is carried through to the last sublevel, and the remaining $2I$ populations are shifted by one level. This means that the sign of the quadrupole interaction can be determined with AFP-ON.

The principle of MAPON is described in detail in Refs. 13 and 14. A MAPON sweep consists of a sequence of *two* AFP sweeps that are separated in frequency by $\Delta \nu$. The influence of the MAPON sweep on the time evolution of the sublevel populations is different for $\Delta \nu > \Delta \nu_{\text{Q}}$ and $\Delta \nu < \Delta \nu_{\text{Q}}$: For a sharp EQI the MAPON spectrum (γ anisotropy as function of $\Delta \nu$) would be a θ function with the step at $\Delta \nu = \Delta \nu_{\text{Q}}$. The distribution of the EQI is determined by differentiation of the MAPON spectrum—in this case a δ function. In reality, the quadrupole interaction is inhomogeneously broadened, which can be described by a Gaussian distribution of the quadrupole subresonance frequencies. The MAPON spectrum is then given by the integral of this distribution, i.e., an error function. The half value of the measured MAPON spectrum is denoted as $\Delta \nu_{\text{Q}}^{(\text{MAP})}$. For the determination of the EQI from $\Delta \nu_{\text{Q}}^{(\text{MAP})}$ several (small) corrections have to be applied. (i) $\Delta \nu_{\text{Q}}^{(\text{sw})}$, due to the finite sweep time of the MAPON sweep with respect to the nuclear spin lattice relaxation time; (ii) $\Delta \nu_{\text{Q}}^{(\text{rf})}$, due to rf power broadening; (iii) 90° geometry only, $\Delta \nu_{\text{Q}}^{(\alpha)}$, due to the unavoidable misalignment of the single-crystal c axis with respect to the direction of B_{ext} [this angle is typically $\alpha = 89.5(5)^\circ$ instead of the exact 90°]; (iv) 90° geometry only, $\Delta \nu_{\text{Q}}^{(\text{Q,M})}$, due to the fact that the principal axes systems of the electric quadrupole interaction and the magnetic interaction are not collinear. All these (generally small) corrections can be determined by model calculations.¹⁵

The time dependence of the MAPON post-passage signal is for $I > 3/2$ different for both sweep directions. This feature can also be used for the determination of the sign of the quadrupole interaction.

IV. EXPERIMENTAL DETAILS

Radioactive ^{82}Br was produced by neutron irradiation of KBr at the reactor FRG-1 in Geesthacht for 3 days in a neutron flux of 6×10^{13} n/cm² s. It was implanted into a hcp Co single crystal at the mass separator in Bonn with an implantation energy of 138 keV. The total impurity dose was 6×10^{12} /cm². The NMR-ON, AFP-ON and MAPON measurements were performed at the ^3He - ^4He -dilution refrigerator in Munich. Two experiments were performed, with the single crystal c axis parallel (0° geometry) and perpendicular (90° geometry) to the direction of the external magnetic field B_{ext} . In 0° geometry, the measurements were performed in zero external magnetic field. In 90° geometry, $B_{\text{ext}} = 15\text{--}18$ kG was applied to force the electronic magnetization parallel B_{ext} .

V. MEASUREMENTS

NMR-ON spectra measured for 0° geometry with $B_{\text{ext}} = 0$ and 90° geometry with $B_{\text{ext}} = 15$ kG are shown in Fig. 1. According to Eq. (8) the magnetic-resonance frequency is

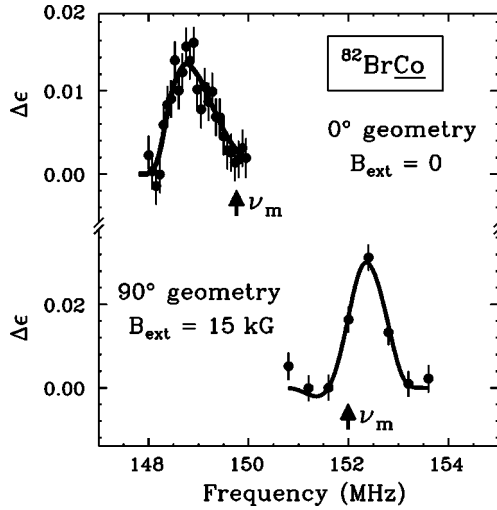


FIG. 1. NMR-ON spectra of $^{82}\text{BrCo}^{(\text{hcp})}$ measured for $M\parallel c$ (top, $B_{\text{ext}}=0$) and $M\perp c$ (bottom, $B_{\text{ext}}=15$ kG). The offset of the magnetic splitting from the resonance center is marked with arrows.

displaced from the observed resonance center by $(\bar{m} + 1/2)\Delta\nu_Q$; therefore the quadrupole interaction must be taken into account for a correct interpretation of the measured NMR-ON spectra.

A MAPON spectrum measured for 0° geometry with $B_{\text{ext}}=0$ (sweep time is 2 s) is shown in Fig. 2. The result is $\Delta\nu_Q^{(\text{MAP})}=287.8(4)$ kHz. The width of the distribution is $\Gamma_{\Delta\nu_Q^{(\text{MAP})}}=6.2(7)$ kHz, i.e., extremely small; the relative width is $\Gamma_{\Delta\nu_Q^{(\text{MAP})}}/\Delta\nu_Q^{(\text{MAP})}\sim 2.2\times 10^{-2}$. It is a remarkable fact that $\Delta\nu_Q^{(\text{MAP})}$ can be determined with an accuracy of 0.4 kHz, for a resonance frequency of ~ 150 MHz. At such a high precision it cannot be excluded *a priori* that the shift due to power broadening can be neglected. To get experimental information on the rf power broadening effect, an additional MAPON spectrum was measured with the same adiabatic factor A : The sweep time was reduced and the rf power was increased, both by a factor of 8. In this way the shift of $\Delta\nu_Q^{(\text{MAP})}$ by the power broadening should increase by a factor of $\sqrt{8}$. The results for this measurement are

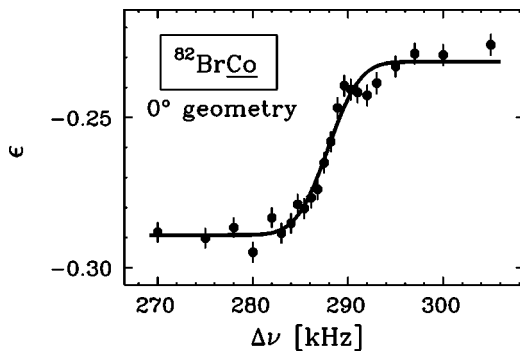


FIG. 2. MAPON spectrum of $^{82}\text{BrCo}^{(\text{hcp})}$ measured for $M\parallel c$. The solid line is the result of a *least-squares* fit, taking into account a Gaussian distribution for the quadrupole subresonance resonance separation. The MAPON signal is given by the integral of this distribution, i.e., an error function with half value at $\Delta\nu_Q^{(\text{MAP})}$ and width $\Gamma_{\Delta\nu_Q^{(\text{MAP})}}$.

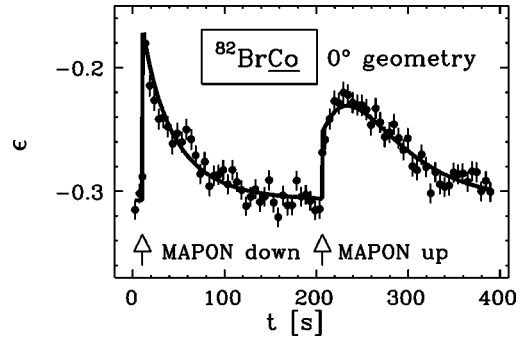


FIG. 3. Sweep-down and sweep-up MAPON post-passage signal for $^{82}\text{BrCo}^{(\text{hcp})}$ with $M\parallel c$. The solid line is the result of a *least-squares* fit with the Korringa constant C_K for the nuclear-spin-lattice relaxation, the adiabatic parameter A for the AFP inversion, and the sign of the EQI as free parameters. The sign of the EQI is uniquely found to be positive.

$\Delta\nu_Q^{(\text{MAP})}=288.0(5)$ kHz, $\Gamma_{\Delta\nu_Q^{(\text{MAP})}}=9.5(1.0)$ kHz. The width is slightly larger; the power-broadening shift even at this higher power level is negligibly small. The shift due to the finite sweep time of the MAPON sweep is estimated to be $\Delta\nu_Q^{(\text{sw})}=+0.05$ kHz, which can be neglected. With the MAPON post-passage signal for both sweep directions—the spectrum is shown in Fig. 3—the sign of the quadrupole splitting is uniquely determined to be positive. Thus, we find $\Delta\nu_Q^{\parallel}=+287.8(4)$ kHz and hence

$$\nu_Q^{\parallel}=+8.634(12) \text{ MHz.}$$

A MAPON spectrum measured for 90° geometry with $B_{\text{ext}}=17$ kG is shown in Fig. 4. The results are $\Delta\nu_Q^{(\text{MAP})}=145.1(9)$ kHz, $\Gamma_{\Delta\nu_Q^{(\text{MAP})}}=17(3)$ kHz. Here the relative width is $\Gamma_{\Delta\nu_Q^{(\text{MAP})}}/\Delta\nu_Q^{(\text{MAP})}\sim 12\times 10^{-2}$, i.e., considerably larger than observed for 0° geometry. At present we cannot give a convincing explanation for the different relative widths. However, such a behavior has been observed for other isotopes also.¹⁵ The sign of the quadrupole splitting was in this case determined with AFP-ON. From the difference of the post-passage signals for sweep up and sweep down (see Fig. 5) it is uniquely found to be negative. Taking now $\Delta\nu_Q^{(\text{MAP})}=-145.1(9)$ kHz and applying corrections as described in Sec. III B of $\Delta\nu_Q^{(\alpha)}=-1.5(1.5)$ kHz, $\Delta\nu_Q^{(\text{QM})}$

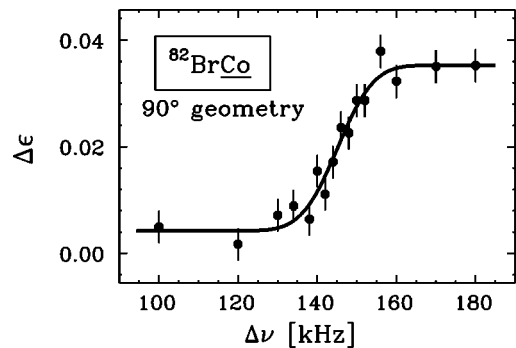


FIG. 4. MAPON spectrum of $^{82}\text{BrCo}^{(\text{hcp})}$ measured for $M\perp c$ ($B_{\text{ext}}=17$ kG).

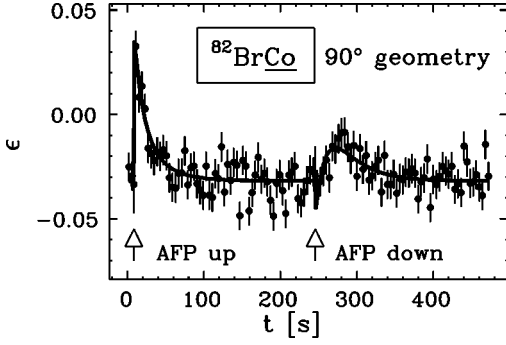


FIG. 5. Sweep-up and sweep-down AFP-ON for $^{82}\text{BrCo}^{\text{(hcp)}}$ with $M \perp c$ ($B_{\text{ext}} = 17$ kG). From the asymmetry of the post-passage signal for the different sweep directions the sign of the EQI is uniquely found to be negative.

$$= -0.5(3) \text{ kHz}, \quad \Delta \nu_Q^{\text{(sw)}} = -0.3(3) \text{ kHz}, \quad \Delta \nu_Q^{\text{(rf)}} = -0.4(6) \text{ kHz}, \text{ the final result is}$$

$$\nu_Q^\perp = -4.43(6) \text{ MHz.}$$

Taking into account the quadrupole-splitting frequencies as obtained from the MAPON measurements the continuous-wave NMR-ON spectra were analyzed (solid curves in Fig. 1). The results for the magnetic hyperfine splitting frequencies (marked with arrows in Fig. 1) are $\nu_M^\parallel(B_{\text{ext}}=0) = 149.76(15)$ MHz and $\nu_M^\parallel(B_{\text{ext}}=15 \text{ kG}) = 151.99(13)$ MHz. For the correct extrapolation of the latter value to $B_{\text{ext}}=0$ the sign of the hyperfine field has to be known. It was determined with measurements of the ν_1 resonance of ^{77}Br in hcp Co in 90° geometry:¹⁵ From $\nu_1^\perp(B_{\text{ext}}=15 \text{ kG}) = 304.20(11)$ MHz and $\nu_1^\perp(B_{\text{ext}}=17 \text{ kG}) = 305.86(13)$ MHz the sign of the hyperfine field is uniquely determined to be positive. Taking for ^{82}Br $d\nu/dB_{\text{ext}} = +0.248(2)$ MHz/kG and taking into account the error introduced by the angular uncertainty of the c axis with respect to B_{ext} in the 90° geometry, we get $\nu_M^\perp(B_{\text{ext}}=0) = 148.40(15)$ MHz. As final results we adopt

$$\nu_M^\parallel(B_{\text{ext}}=0) = 149.76(15) \text{ MHz,}$$

$$\nu_M^\perp(B_{\text{ext}}=0) = 148.40(15) \text{ MHz.}$$

Our value for $\nu_M^\parallel(B_{\text{ext}}=0)$ is slightly larger than 148.9(2) MHz reported by Dämmrich and Herzog.¹⁶

A relaxation spectrum measured for 0° geometry with $B_{\text{ext}}=0$ is shown in Fig. 6. The result for the Korringa constant is $C_K = 1.27(12)$ K s. From a second measurement we get $C_K = 1.38(18)$ K s. Taking into account the results for C_K from the MAPON and AFP-ON measurements we adopt as a final result

$$C_K = 1.30(10) \text{ K s.}$$

VI. RESULTS AND DISCUSSION

With the magnetic hyperfine splitting frequencies given in Sec. V we get, taking $\mu = 1.6270(5)\mu_N$,¹⁷ for the hyperfine fields,

$$B_{\text{HF}}^\parallel = +603.77(63) \text{ kG,}$$

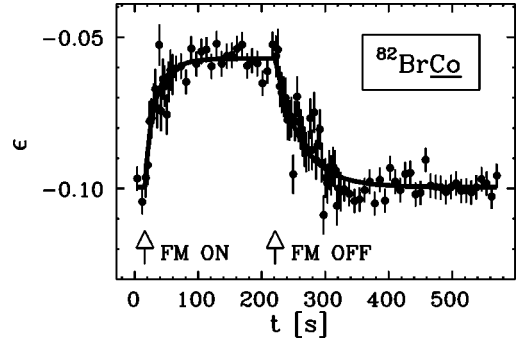


FIG. 6. Time dependence of the γ anisotropy after resonant depolarization (FM on) and return to the thermal-equilibrium value (FM off) for $^{82}\text{BrCo}^{\text{(hcp)}}$ with $M \parallel c$ and $B_{\text{ext}}=0$.

$$B_{\text{HF}}^\perp = +598.29(63) \text{ kG.}$$

The isotropic and anisotropic contributions are

$$B_{\text{HF}}^{\text{(iso)}} = +600.12(63) \text{ kG,}$$

$$B_{\text{HF}}^{\text{(ani)}} = +3.65(60) \text{ kG.}$$

The hyperfine fields in hosts Fe, Ni, and hcp Co of the elements between $Z=31$ and 36 —this is one of the regions where the hyperfine fields are positive—are listed in Table I. The sign of the hyperfine fields in hcp Co is the same as for Fe and Ni as host lattice, the characteristic dependence on Z being qualitatively similar. For bromine in hcp Co the ratio $B_{\text{HF}}^{\text{(ani)}}/B_{\text{HF}}^{\text{(iso)}} = +0.62(10) \times 10^{-2}$ is different in magnitude and sign from the corresponding ratio for the pure system $\text{CoCo}^{\text{(hcp)}} [-2.37(4) \times 10^{-2}]$. This means that both $B_{\text{HF}}^{\text{(iso)}}$ and $B_{\text{HF}}^{\text{(ani)}}$ are element-specific and can thus be taken for meaningful tests of future theoretical calculations.

Taking $Q = +0.748(10)$ b,^{17,4} we get for the principal components of the EFGs

$$V_{zz}^{\text{(ani)}} = +0.476(6) \times 10^{17} \text{ V/cm}^2,$$

$$V_{zz}^{\text{(iso)}} = -0.004(2) \times 10^{17} \text{ V/cm}^2.$$

TABLE I. Hyperfine fields in Fe, Ni, and hcp Co.

Z	Element	$B_{\text{HF}}^{\text{(Fe)}}$ (kG)	$B_{\text{HF}}^{\text{(Ni)}}$ (kG)	$B_{\text{HF}}^{\text{(hcp Co)}}$ (kG)
31	Ga	-110(3) ^a	-12.5(2.1) ^b	-81.5(3) ^c
32	Ge	+70(3) ^d	+38.8(1.2) ^e	+46.5(20) ^e
33	As	+343.9(3) ^f	+106(2) ^g	+274(6) ^c
34	Se	+690(50) ^h	+151.1(3.5) ⁱ	(+)420(40) ^h
35	Br	+813.1(8) ^j	+80(1) ^k	+600.12(63) ^l
36	Kr	+660(270) ^m	-7(1) ^k	

^aReference 18.

^bReference 5.

^cReference 27.

^dReference 19.

^eReference 24.

^fReference 20.

^gReference 25.

^hReference 21.

ⁱReference 26.

^jReference 22.

^kReference 9.

^lThis work.

^mReference 23.

Let us first discuss the isotropic EFG. (Here and in the following “EFG” is used for “principal component of the traceless EFG tensor.”) For the pure system $\text{CoCo}^{(\text{hcp})}$ Fekete *et al.*²⁸ showed that an isotropic contribution to the EFG exists, which has been ascribed to the relativistic contribution of the d band to the electronic-field gradient at the ^{59}Co site. The origin of this type of EFG is the spin-orbit interaction. In addition to the pure system $\text{CoCo}^{(\text{hcp})}$, a SO-EFG in hcp Co is known at present only for $5d\text{IrCo}^{(\text{hcp})}$.²⁹ Recently it was found that the SO-EFG for Ir in hcp Co is relatively large, whereas it is at least two orders of magnitude smaller for Pt and Hg—the experimental SO-EFG’s for Pt and Hg are consistent with zero. For Br, the result for the isotropic EFG indicates that it might be slightly different from zero; within two standard deviations, however, zero is included. In any case, it is at least about two orders of magnitude smaller than the anisotropic EFG.

The lattice contribution to the EFG in hcp Co is positive; all hitherto known EFG’s are, however, negative. For the pure system $\text{CoCo}^{(\text{hcp})}$ Fekete *et al.*²⁸ explain this with the empirical rule of Raghavan *et al.* for nonmagnetic noncubic metals, according to which the EFG is given by

$$V_{zz} = (1 - K)V_{zz}^{(\text{latt})}(1 - \gamma_{\infty}), \quad (11)$$

where K is a “universal” constant, $K = +3$,³⁰ and $(1 - \gamma_{\infty})$ takes into account the electronic shielding (antishielding) of the EFG at the nuclear site (Sternheimer effect). In this way, the negative signs of the presently known EFG’s of impurity-hcp-Co systems are also plausible. For Br, the free-atom shielding factors depend on the electronic configuration: According to calculations by Feiock and Johnson,³¹ $\gamma_{\infty} = -5.9$, $+834.6$, and -210.0 for $(4p_{1/2})^0$, $(4p_{1/2})^2$, and $(4p_{1/2})^2(4p_{3/2})^4$, respectively. This means that the electronic configuration of Br in hcp Co must be dominated by $(4p_{1/2})^2$, by which the positive sign of the EFG would be

TABLE II. Reduced relaxation rates in hcp Co.

Element	R_K/ν_M^2 [10^{-17} s/K)	Ref.
Co	12.2(7)	32
Br	3.4(3)	This work
Zr	1.22(9)	15
Nb	1.13(12)	15
Rh	1.52(4)	15

explained plausibly. Consequently, the bromine ions in the metal cobalt should be in the core electronic configuration $3+$ close to the electronic configuration of cobalt itself.

For a comparison of the relaxation of different impurities it is convenient to quote the reduced relaxation rate R_K/ν_M^2 , where $R_K = 1/C_K$. For Br in hcp Co it is

$$R_K/\nu_M^2 = 3.4(3) \times 10^{-17} \text{ s/K}.$$

The reduced relaxation rates for Co, Br, Zr, Nb, and Rh in hcp Co are listed in Table II. The faster relaxation of Co with respect to Zr, Nb, and Rh is probably due to a process involving the $3d$ electrons.⁷ This mechanism is missing for Br. Compared with Zr, Nb, and Rh, the relaxation for Br is by a factor of ~ 3 faster. The faster relaxation indicates a higher density of electrons at the Fermi energy that could be connected with the core electronic configuration $3+$.

ACKNOWLEDGMENTS

We wish to thank E. Smolic for experimental help. The support of the Forschungszentrum Geesthacht, Zentralabteilung Forschungsreaktoren, in the production of ^{82}Br is acknowledged. This work was funded by the Deutsche Forschungsgemeinschaft (DFG) under Contract Nos. Ha 1282/3-3 and He 1316/3-1.

¹B. Hinfurtner, E. Hagn, E. Zech, R. Eder, and the NICOLE and ISOLDE Collaboration, Phys. Rev. Lett. **67**, 812 (1991).

²G. Seewald, E. Hagn, B. Hinfurtner, E. Zech, D. Forkel-Wirth, R. Eder, and ISOLDE Collaboration, Phys. Rev. Lett. **77**, 5016 (1996).

³G. Seewald, E. Hagn, E. Zech, I.P. Johnstone, I.S. Towner, D. Forkel-Wirth, and ISOLDE Collaboration, Phys. Rev. Lett. **80**, 924 (1998).

⁴G. Seewald, E. Hagn, E. Zech, K. Freitag, P. Herzog, D. Forkel-Wirth, and ISOLDE Collaboration, Phys. Rev. Lett. **80**, 5289 (1998).

⁵G.N. Rao, Hyperfine Interact. **24-26**, 1119 (1985).

⁶M. Akai, H. Akai, and J. Kanamori, J. Phys. Soc. Jpn. **54**, 4246 (1985); **54**, 4257 (1985).

⁷J. Kanamori, H. Yoshida, and K. Terkura, Hyperfine Interact. **9**, 363 (1981).

⁸P.H. Dederichs, R. Zeller, H. Akai, S. Blügel, and A. Oswald, Philos. Mag. B **51**, 137 (1985).

⁹S. Seeger, H.H. Bertschat, R. Kowallik, H. Waldmann, W.-D. Zeitz, D. Forkel-Wirth, H. Haas, and ISOLDE Collaboration, Phys. Lett. A **201**, 349 (1995).

¹⁰E. Hagn, Phys. Rev. B **25**, 1521 (1982).

¹¹E. Matthias and R. J. Holliday, Phys. Rev. Lett. **17**, 897 (1966).

¹²K.S. Krane, in *Low-Temperature Nuclear Orientation*, edited by N.J. Stone and H. Postma (North-Holland, Amsterdam, 1986), p. 31.

¹³P.T. Callaghan, P.J. Back, D.H. Chaplin, H.R. Foster, and G.V.H. Wilson, Hyperfine Interact. **22**, 39 (1985).

¹⁴P.T. Callaghan, P.J. Back, and D.H. Chaplin, Phys. Rev. B **37**, 4900 (1988).

¹⁵G. Seewald, Ph.D. thesis, TU München, 1999.

¹⁶U. Dämmrich and P. Herzog, Hyperfine Interact. **43**, 169 (1988).

¹⁷P. Raghavan, At. Data Nucl. Data Tables **42**, 189 (1989).

¹⁸M. Kontani and J. Itoh, J. Phys. Soc. Jpn. **22**, 345 (1967).

¹⁹J. Morgenstern, J.W. Schmidt, G. Flugge, and H. Schmidt, Phys. Lett. **27B**, 379 (1968).

²⁰Y. Koi, M. Kawakami, T. Hihara, and A. Tsujimura, J. Phys. Soc. Jpn. **33**, 267 (1972).

²¹P.T. Callaghan, N.J. Stone, and B.G. Turrel, Phys. Rev. B **10**, 1075 (1974).

²²P. Herzog, U. Dämmrich, K. Freitag, C.-D. Herrmann, and K. Schlösser, Z. Phys. B **64**, 353 (1986).

- ²³A.V. Aldushehenkov and A.G. Serfeev, *Zh. Éksp. Teor. Fiz.* **62**, 581 (1975).
- ²⁴P. Raghavan, M. Senba, and R.S. Raghavan, *Hyperfine Interact.* **4**, 330 (1978).
- ²⁵H. Bertschat, G. Echt, H. Haas, E. Recknagel, E. Schlodder, and B. Spellmeyer, *Hyperfine Interact.* **1**, 251 (1975).
- ²⁶M. Mohsen and F. Pleiter, *Hyperfine Interact.* **39**, 123 (1988).
- ²⁷P. Raghavan, M. Senba, and R.S. Raghavan, *Phys. Rev. Lett.* **39**, 1547 (1977).
- ²⁸D. Fekete, H. Boasson, A. Grayevski, V. Zevin, and N. Kaplan, *Phys. Rev. B* **17**, 347 (1978).
- ²⁹G. Seewald, B. Hinfurtner, E. Hagn, E. Zech, D. Forkel-Wirth, R. Eder, and ISOLDE Collaboration, *Phys. Rev. Lett.* **80**, 3638 (1998).
- ³⁰P. Raghavan, E.N. Kaufmann, R.S. Raghavan, E.J. Ansaldo, and R.A. Naumann, *Phys. Rev. B* **13**, 2835 (1976).
- ³¹F.D. Feiock and W.R. Johnson, *Phys. Rev.* **187**, 39 (1969).
- ³²H. Enokiya, *J. Phys. Soc. Jpn.* **42**, 796 (1977).